

CAN THE COSMIC-RAY DRIVEN DYNAMO MODEL EXPLAIN THE OBSERVATIONS OF THE POLARIZED EMISSION OF EDGE-ON GALAXIES ?

KATARZYNA OTMIANOWSKA-MAZUR¹, MARIAN SOIDA¹, BARBARA KULESZA-ŻYDZIK¹, MICHAŁ HANASZ³, AND GRZEGORZ KOWAL²

Draft version December 11, 2008

ABSTRACT

In the present paper we construct maps of polarized synchrotron radio emission of a whole galaxy, based on local models of the cosmic ray (CR) driven dynamo. We perform numerical simulations of the dynamo in local Cartesian domains, with shear-periodic boundary conditions, placed at the different galactocentric radii. Those local solutions are concatenated together to construct the synchrotron images of the whole galaxy. The main aim of the paper is to compare the model results with the observed radio continuum emission from nearly edge-on spiral galaxy.

On the basis of the modeled evolution of the magnetic field structure, the polarization maps can be calculated at different time-steps and at any orientation of the modeled galaxy. For the first time a self-consistent cosmic-ray electron distribution is used to integrate synchrotron emissivity along the line of sight. Finally, our maps are convolved with the given radiotelescope beam. We show that it is possible to reconstruct the extended magnetic halo structures of the edge-on galaxies (so called X-shaped structures).

Subject headings: ISM: galactic dynamo — magnetic field — radio polarized emission

1. INTRODUCTION

Recent deep observations of polarized radio-continuum emission at centimeter wavelengths of edge-on spiral galaxies (Tüllmann et al. 2000; Soida 2005; Heesen et al. 2005) revealed characteristic X-shaped magnetic field structure. Many galaxies showed magnetic field oriented in the halo at a large angle to the galaxy disk. Earlier observations, mostly limited by sensitivity to narrow area along the major axis, demonstrated mainly plane-parallel component (e.g. Dumke et al. 1995). The polarization vectors of NGC 5775 close to the galactic plane are parallel to the disk, but in the halo they extend up to 10 kpc above the disk forming so called X-shaped structure in all four quadrants. Such picture most probably reflects the quadrupole configuration of magnetic field in NGC 5775 Soida et al. (2008). The observed degree of polarization is very high (locally reaching even up to 50%). It resembles high regularity of magnetic field there. Such structures seem to be common among edge-on spiral galaxies (NGC 5775, NGC 4666, NGC 4217 NGC 3628, NGC 253, NGC 891, (see e.g. Dahlem et al. 1997; Sukumar & Allen 1991; Soida 2005). In addition, Tüllmann et al. (2000) detected that NGC 5775 shows differential rotation in the direction perpendicular to the disk. So far, there is no physical explanation for those extended structures.

An attempt to explain the structure of polarized vectors by the dipolar dynamo wave in the NGC 5775 was made by Sokoloff (2002). He used a solution of the dipolar classical turbulent dynamo equation and as a result he got structures not confirmed by the observations so

far Soida et al. (2008).

The principle of the action of the CR-driven dynamo (Parker 1992; Hanasz & Lesch 2000; Hanasz et al. 2004) is based on the cosmic ray (CR) energy supplied continuously by supernova (SN) remnants. Due to the anisotropic diffusion of cosmic rays along the horizontal magnetic field lines, cosmic rays tend to accumulate within the disc volume. However, the configuration stratified by the vertical gravity is unstable against the Parker instability. Buoyancy effects induce the vertical and horizontal motions of the fluid and the formation of undulatory patterns – magnetic loops in the frozen-in, predominantly horizontal magnetic fields. The presence of rotation in galactic disks implies a coherent twisting of the loops by means of the Coriolis force leading to the generation of the small-scale radial magnetic field components. The next phase is merging the small-scale loops by the magnetic reconnection process which forms the large scale radial magnetic fields. Finally, the differential rotation stretches the radial magnetic field amplifying the large-scale azimuthal magnetic field. The coupling of amplification processes of the radial and azimuthal magnetic field components results in exponential growth of the large scale magnetic field with timescales of galactic rotation period (140 Myr) as shown by Hanasz et al. (2006).

In this paper we present the results of galactic disk modeling which is constructed from a set of local volumes placed at different distances from the galactic center. We show the results of integration of synchrotron emissivities (Stokes parameters I, Q and U) along the line of sight (LOS), and compare them to the observed radio images of the galaxy NGC 5775. Our results are compared to polarized radio continuum observations made at 6 cm (Tüllmann et al. 2000).

2. MODELS OF THE COSMIC-RAY DRIVEN DYNAMO

¹ Astronomical Observatory, Jagiellonian University, ul. Orła 171, 30-244 Kraków, Poland

² Department of Astronomy, University of Wisconsin, 475 North Charter Street, Madison, WI 53706, USA

³ Toruń Centre for Astronomy, Nicolaus Copernicus University, ul. Gagarina 11, 87-100 Toruń, Poland

The first complete 3D numerical model of the CR-driven dynamo has been demonstrated by Hanasz et al. (2004, 2005, 2006); Otmianowska-Mazur et al. (2007). Our model of the cosmic ray driven dynamo includes the following physical elements: the ionized gas and magnetic field described by resistive MHD equations, the cosmic ray component described by the diffusion-advection transport equation (see Hanasz & Lesch 2003, for the details of the numerical algorithm), cosmic rays diffusing anisotropically along magnetic field lines (Giacalone & Jokipii 1999; Jokipii et al. 1999), supernova remnants exploding randomly in the disk volume, the finite (currently uniform) resistivity of the ISM (see Hanasz et al. 2002; Hanasz & Lesch 2003; Kowal, Hanasz & Otmianowska-Mazur 2003; Tanuma et al. 2003) and the realistic vertical disk gravity and rotation (Ferrière 1998). In the present models gas motions arise only from the cosmic-ray pressure gradients. We neglect any shock effects, like gas heating. It is caused by limitations of currently used explicit algorithm for cosmic ray diffusion, although we plan to incorporate shock effects in our future papers. A complementary work incorporating effects of dynamo powered directly by supernova-driven turbulence, but without taking into account the cosmic rays, has been recently published by Gressel et al. (2008a,b). In the present paper we attempt to examine observational properties of our model of cosmic ray-driven dynamo.

The system of coordinates x, y, z corresponds locally to the global galactic cylindrical system r, ϕ, z . The boundary conditions are periodic in the Y-direction, sheared in the X-direction (following Hawley et al. 1995) and open in the Z-direction for fluid quantities and magnetic field components. The boundary conditions for cosmic rays are fixed ($e_{cr} = 0$) on the Z-boundaries.

We present a new set of numerical models of the CR-driven dynamo computed in cubes situated at different distances from the center of the galaxy (see Fig. 1). We intend to obtain the picture of the whole galaxy from these local cubes. In the inner part of the galaxy a variety of different physical mechanisms occur (such as central activity, bulge influence etc.), most of which are not taken into account by our model. For this reason, we start our calculations at 2 kpc radius. The physical parameters used in the calculations are assumed according to the paper of Ferrière (1998) which refers to the Milky Way (see Fig. 1). Our numerical simulations are performed using the Zeus-3D MHD code (Stone & Norman 1992a,b) with the cosmic rays extension made by Hanasz & Lesch (2003).

The full set of equations describing the model includes the set of resistive MHD equations completed by the cosmic ray transport equation (see Hanasz et al. 2004)

$$\frac{\partial \rho}{\partial t} + \nabla \cdot (\rho V) = 0, \quad (1)$$

$$\frac{\partial e}{\partial t} + \nabla \cdot (eV) = -p(\nabla \cdot V), \quad (2)$$

$$\begin{aligned} \frac{\partial V}{\partial t} + (V \cdot \nabla)V = & -\frac{1}{\rho} \nabla \left(p + p_{cr} + \frac{B^2}{8\pi} \right) \\ & + \frac{B \cdot \nabla B}{4\pi\rho} - 2\Omega \times V + 2q\Omega^2 x \hat{e}_x + g_z(z) \hat{e}_z, \end{aligned} \quad (3)$$

$$\frac{\partial B}{\partial t} = \nabla \times (V \times B) + \eta \Delta B, \quad (4)$$

$$p = (\gamma - 1)e, \quad \gamma = 5/3 \quad (5)$$

where $q = -d \ln \Omega / d \ln R$ is the shearing parameter, (R is the distance to galactic center), η is the resistivity, γ is the adiabatic index of thermal gas, the gradient of cosmic ray pressure ∇p_{cr} is included in the equation of motion (see Berezhinskii et al. 1990, e.g.) and other symbols have their usual meaning. The uniform resistivity is included only in the induction equation (see Hanasz et al. 2002). The thermal, ionized gas component is treated as an adiabatic medium.

The transport of the cosmic ray component is described by the diffusion-advection equation

$$\frac{\partial e_{cr}}{\partial t} + \nabla \cdot (e_{cr} V) = \nabla \cdot (\hat{K} \nabla e_{cr}) - p_{cr} (\nabla \cdot V) + Q_{SN}, \quad (6)$$

where Q_{SN} represents the source term for the cosmic ray energy density: the rate of production of cosmic rays injected locally in SN remnants and

$$p_{cr} = (\gamma_{cr} - 1)e_{cr}, \quad \gamma_{cr} = 14/9. \quad (7)$$

The adiabatic index of the cosmic ray gas γ_{cr} and the formula for diffusion tensor

$$K_{ij} = K_{\perp} \delta_{ij} + (K_{\parallel} - K_{\perp}) n_i n_j, \quad n_i = B_i / B, \quad (8)$$

are adopted following the argumentation by Ryu et al. (2003).

In order to construct the polarization maps of an edge-on galaxy characterized by a high halo, our local simulation is extended to 4 kpc above and below the disk. The local cube X-size is 500 pc, while Y-size is 1000 pc. The cell sizes are equal to $dx=dy=dz=20$ pc. The resolution of our local calculations is given by $25 \times 50 \times 400$ grid points. However, we are primarily interested in the large scale magnetic field amplification and structure. Because CR gas propagates diffusively and gas dynamics does not involve shock waves, the currently assumed grid resolution is sufficient. This statement is verified by resolution studies - simulations performed with the cell size $(10 \text{ pc})^3$ up to $(20 \text{ pc})^3$ lead to convergent results.

The disk rotation was defined by the values of the angular velocity Ω at the different galactocentric radii ranging from 0.05 Myr^{-1} at $R_G = 5 \text{ kpc}$ down to 0.025 Myr^{-1} at $R_G = 10 \text{ kpc}$ (see. Fig. 1). The value of the shearing parameter is $q = 0$ up to a radius of 3 kpc, and linearly increasing to $q = 1$ at 5 kpc, as it is presented in Fig. 1. The cosmic ray diffusion coefficients assumed in the simulations are: $K_{\parallel} = 3 \times 10^{27} \text{ cm}^2 \text{ s}^{-1}$ and $K_{\perp} = 3 \times 10^{26} \text{ cm}^2 \text{ s}^{-1}$. These values are scaled down by an order of magnitude with respect to expected realistic values (e.g. Jokipii et al. 1999) due to the timestep limitation in the currently used explicit algorithm for the diffusion equation. The assumed value of the resistivity coefficient η is $3 \times 10^{25} \text{ cm}^2 \text{ s}^{-1}$. The values of other input parameters are depicted in Fig. 1.

3. CONSTRUCTION OF SYNTHETIC RADIO MAPS

As the result of our local calculations we obtained 3D rectangular cubes of the magnetic field and the cosmic-ray energy density. Since the CR component is described

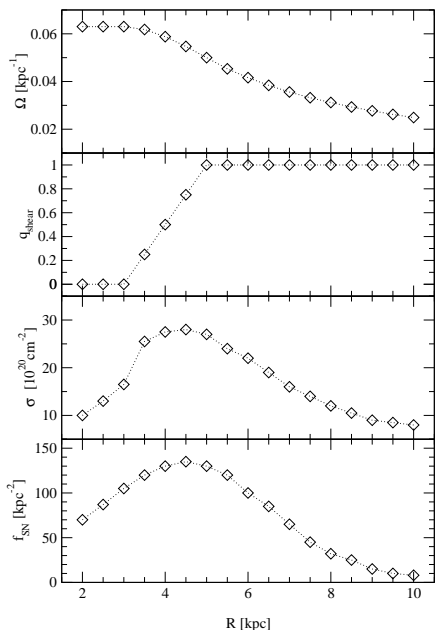


FIG. 1.— Radially dependent parameters for all our local calculations. Subsequent panels (counting from the top) display angular velocity Ω , shearing parameter q_{shear} , gas column density σ and supernova rate f_{SN} , vs. galactocentric radius R_G , deduced from the model by Ferriere (1998).

as adiabatic relativistic gas instead of the full momentum distribution function, the energy density of cosmic rays can be considered as proportional to the number density of CR nucleons. The number density of cosmic ray electrons $n_{e,cr}$ is typically assumed to be of the order of 1 % of the number density of cosmic ray nucleons $n_{n,cr}$. Therefore $n_{e,cr}$ can be assumed proportional to e_{cr} . The local cubes at given radius and chosen time-step are replicated into subsequent cylinders, and cylinders are combined together into the full galactic disk (at the radii 2 – 10 kpc, and of 8 kpc thickness). The synthesized disk can be oriented according to the inclination and position angle of any real galaxy (in the case of NGC 5775 it is 86° and 145° , respectively). After computing the magnetic field component perpendicular to the line of sight B_\perp and relativistic-electron density $n_{e,cr}$ from the simulation data we calculate the synchrotron emissivity at each point. Following the standard formula (see e.g. Longair 1994) we obtain Stokes parameters I, Q, and U:

$$\frac{d}{dl} \begin{pmatrix} I \\ Q \\ U \end{pmatrix} = \begin{pmatrix} \epsilon_I & 0 & 0 \\ p\epsilon_I \cos 2\chi & \cos \Delta & -\sin \Delta \\ p\epsilon_I \sin 2\chi & \sin \Delta & \cos \Delta \end{pmatrix} \begin{pmatrix} I \\ Q \\ U \end{pmatrix}, \quad (9)$$

where the synchrotron emissivity is

$$\epsilon_I \propto n_{e,cr} B_\perp^{(\gamma+1)/2} \propto e_{cr} B_\perp^{(\gamma+1)/2}, \quad (10)$$

and Δ denotes the Faraday rotation angle. Integrating the Stokes parameters along the line of sight we obtain the map of synchrotron emission of the simulated galaxy. We set $\gamma = 2.8$ and $p = 75\%$.

In addition, assuming that the distribution of thermal electrons $n_{e,th}$ is proportional to the gas density, we can

account for the Faraday rotation of polarized emission along the line of sight. The Faraday rotation in small distance dl is

$$\Delta \propto n_{e,th} B_\parallel dl. \quad (11)$$

Finally, we convolve resulting I, Q, and U maps with Gaussian beam of HPBW of $20''$ and calculate polarized intensity and vectors of magnetic polarization (B) for direct comparison with real observations of NGC 5775.

4. RESULTS

The evolution of the magnetic field energy, the cosmic ray energy and the mean values of the magnetic pitch angles calculated in the subsequent rings for five chosen distances from the galactic center is presented in Fig. 2.

In all local models with nonvanishing differential rotation ($q_{shear} \neq 0$) i.e. at the radii $R > 3 \text{ kpc}$, a fast growth of the total magnetic field energy is observed (see Fig. 2, – top panel). Within the ring $R = 4\text{--}5 \text{ kpc}$ the mean growth time of the large-scale magnetic field, measured in the phase of exponential amplification of the magnetic field (since $t = 0.2 \text{ Gyr}$ till $t = 0.9 \text{ Gyr}$) is the shortest – about 0.15 Gyr. The growth time gradually increases with the radius up to about 0.3 Gyr for the outermost distance from the galactic center $R = 10 \text{ kpc}$. The fastest growth of the magnetic energy at 4.5 kpc coincides with the largest SN rate and high shear in comparison with other disk areas. For the smallest radii ($R < 3 \text{ kpc}$), with assumed rigid rotation, the magnetic field is not amplified. This justifies our decision of not taking into consideration rings close to the center of the galaxy.

After the exponential amplification phase the magnetic field energy enters the saturation phase – the earlier, the quicker growth rate was observed. The fastest growth of the CR energy (see Fig. 2 – middle panel) is present at the radius 4.5 kpc (solid line) due to the presence of the highest SN rates there, similarly to the magnetic field energy behavior at this galactocentric distance. In our simulations we do not obtain the energy equipartition between the cosmic rays and the magnetic field. The CR energy exceeds the magnetic energy by 1 ÷ 2 orders of magnitude. Possible reasons for this excess are: the low values of the CR diffusion coefficients, as well as, periodic boundary conditions (see Hanasz et al. 2008, for more detailed discussion). The bottom graph in Fig. 2 shows the time evolution of the mean magnetic pitch angles at the same radii as for the magnetic field and the cosmic ray energies. In the beginning stage of evolution (until 0.2 Gyr) all curves exhibit maxima up to 10° . Then, at two distances from the galactic center, 4.5 kpc and 6 kpc, the values of the mean magnetic pitch angles change sign to the negative ones. In the end, after 800 Myr, the pitch angles change again sign to positive values and stabilize for all curves above 5° .

Fig. 3 shows the radial dependency of the magnetic field energy (top panel), the cosmic rays energy (middle panel), and the mean pitch angle values (bottom panel) for four chosen time steps. We notice that the magnetic field energy grows with time and decreases with the radius, as we present in the Figure above. In addition, all curves (Fig 3, the middle panel) showing the radial dependence of the cosmic ray energy exhibit the maxima in their central parts (3–4 kpc). The highest increase is observed for times between 1.5 and 2 Gyr and for the

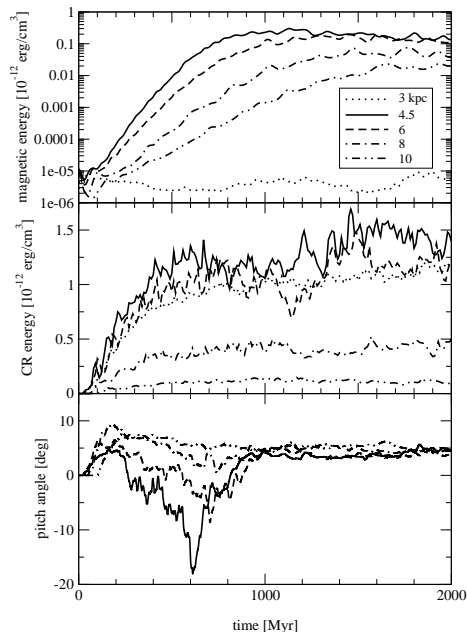


FIG. 2.— Evolution of the magnetic field energy, the CR energy and the mean pitch angle values at five chosen distances (R) from the galactic center: 3 kpc (the dotted lines), 4.5 kpc (the solid lines), 6 kpc (the dashed lines), 8 kpc (the dot-dashed lines), and 10 kpc (the double dot-dashed lines)

radius about 4.5 kpc. As we explained above, the CR energy maxima are connected with the largest rate of SN between 4 and 5 kpc (see Fig. 1).

Due to small shear in the central part (see Fig. 1), the mean magnetic pitch angle (Fig. 3, bottom) reaches the highest values for all chosen time steps. The smallest or negative pitch angle values are obtained at time 0.5 Gyr at the radius 4.5 kpc (like in Fig. 2 – bottom panel). We can conclude that when the dynamo is still under development the pitch angles are low or even negative. Later on, when the energy grows the pitch angles attains about 5° for all radii.

The main goal of this paper is to compare the radio continuum emission obtained from the cosmic ray dynamo model with the observed map of a real galaxy. In Fig. 4 we present the face-on view of our model map at the final time of 2 Gyr. The figure shows polarization vectors superimposed onto the contours and grayplot of the polarized intensity. We see that the central part exhibits the highest pitch angle values. Further out smaller pitch angles are observed, in agreement with the bottom panels of Figs. 2 and 3. This fact can be explained by the lower shear in the galactic center than outward in the disk.

Fig. 5 shows calculated maps of the vectors of the polarized emission superimposed onto the isolines and grayplots of the same quantity with orientation on the sky-plane as the spiral galaxy NGC 5775 (inclination of 86° and position angle of 145°) at selected time steps. One can notice that the extended structures of the polarization vectors in the modeled galaxy are present from the early stages (500 Myr) of the evolution. They appear at

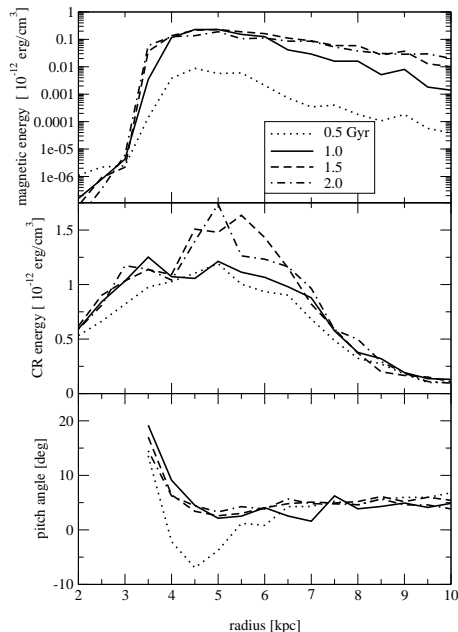


FIG. 3.— Radial dependency of the magnetic field energy, the cosmic ray energy and the mean pitch angle values for four chosen time steps: 0.5 Gyr (dotted lines), 1 Gyr (solid lines), 1.5 Gyr (dashed lines), and 2 Gyr (dot-dashed lines).

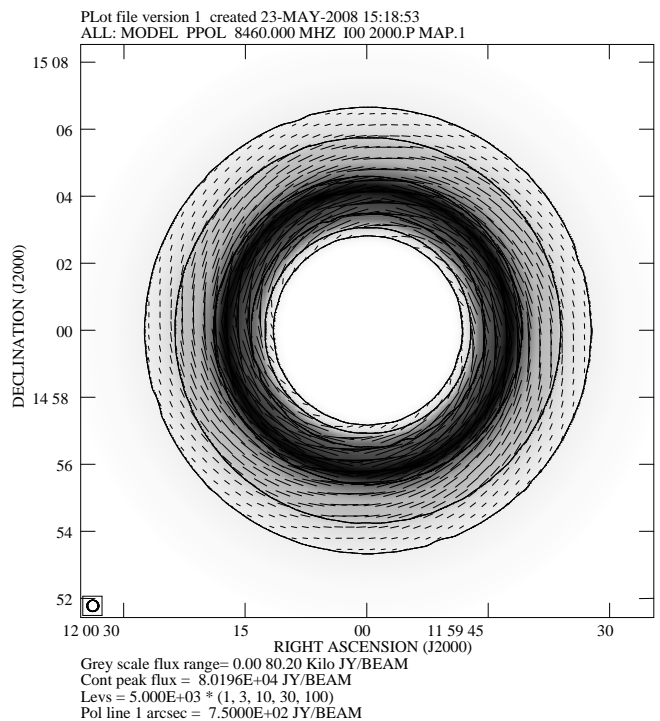


FIG. 4.— Face-on map of the polarized emission of the modeled galaxy. Contours and gray scale show polarized emission intensity, vectors are of directions of apparent magnetic polarization vector, and length proportional to the intensity

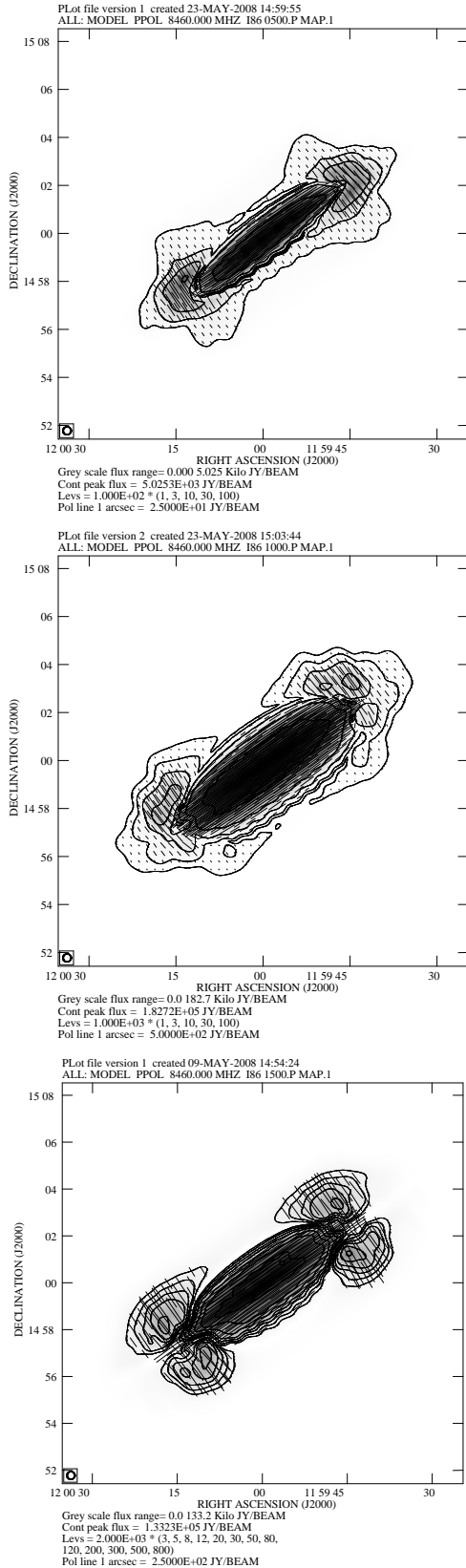


FIG. 5.— Polarization maps of the modeled galaxy at selected time steps: 500 Myr (top panel), 1000 Myr (middle panel), and 1500 Myr (bottom panel) oriented as the real galaxy NGC 5775. Contours and gray scale show polarized emission intensity, vectors are of directions of apparent magnetic polarization vector, and length proportional to the intensity

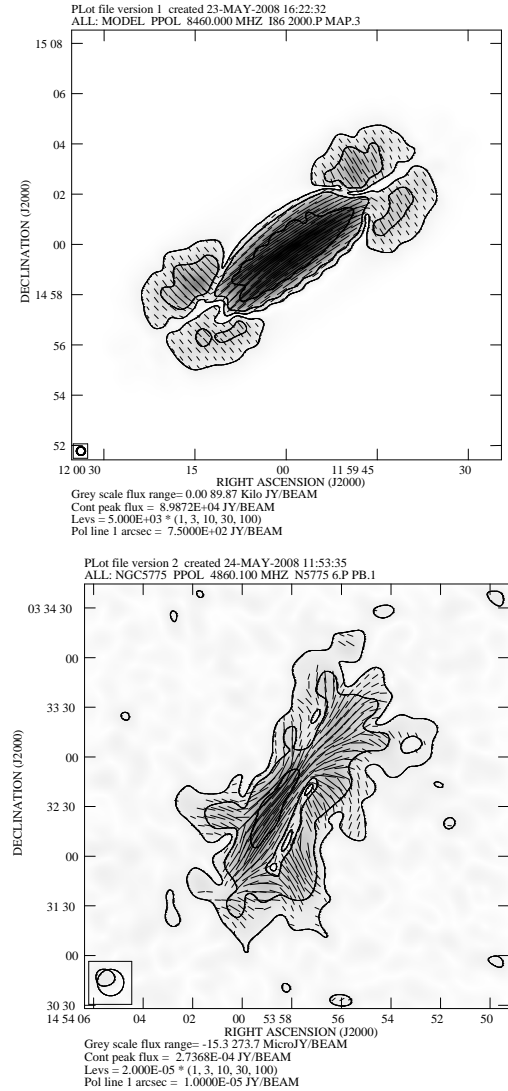


FIG. 6.— Map of the modeled galaxy at the latest (2 Gyr) time-step of the evolution (upper panel) oriented as the real galaxy NGC 5775 (lower panel). Contours and gray scale show polarized emission intensity, vectors are of directions of apparent magnetic polarization vector, and length proportional to the intensity

large distances from the disk forming an X-shaped structure, similarly to the observed map of the polarization emission of the edge-on galaxies. The most extended structures are apparent at the late time steps of our simulations 1500 Myr (the bottom panel) and 2000 Myr (see Fig. 6, the top panel).

In Fig. 6 we compare maps of polarized emission for NGC 5775 (the lower panel) and synthetic maps for our model of this galaxy (the upper panel). In both pictures, isolines of polarized intensity are superimposed onto the grayplot of the same quantity, together with the vectors of directions of the apparent magnetic polarization with the length proportional to the intensity. The polarization vectors in the central part of the bodies are parallel to the disk in both modeled and real galaxies. The extended structures, polarized perpendicularly to the disk plane, are visible in both maps as well. However, in the real NGC 5775 the extensions are separated less than in our model. The depolarized canals, clearly seen in the

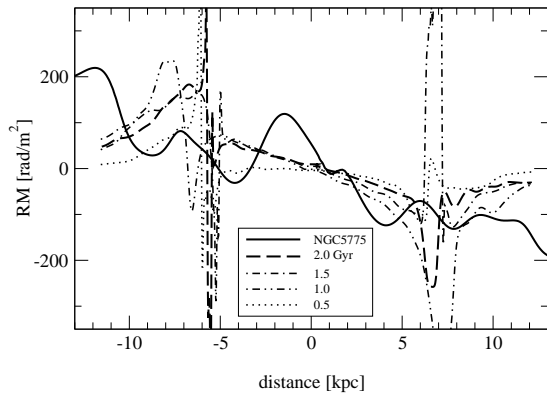


FIG. 7.— Rotation measure plot along the major axis of the galaxy – calculated from the model at four time steps and the real observations of NGC 5775. Negative distances denotes left (south-eastern) side of the galaxy

model map are barely visible in eastern and western extensions in the real galaxy. This suggests that in the real galaxy the magnetic field changes its orientation more smoothly than in the model. Clear differences between the model and real observations appear close to the major axis of the galaxy. Narrow depolarized channel is seen on the lower panel of Fig. 6. It can be explained by relatively strong Faraday effects caused by non-axisymmetric magnetic field configuration present in the front side (the south-western side) close to the disk plane (Soida 2005). Another reason for this behavior could be connected to a local enhancement of magnetic field and/or thermal electron density due to the influence of a spiral arm. Our model does not include any non-axisymmetric features. Furthermore we do not include the very central part in our modeled galaxy. This results in dumping magnetic field at the radii $R < 3$ kpc. In real galaxies any non-axial (vertical) motions can strongly affect magnetic field configuration.

We compare our model with observations at relatively high frequency (4.86 GHz), where Faraday effects usually are small. Nevertheless we include such effects in our calculation of Stokes parameters (Eq. 9). Calculating model maps of polarized emission (intensity and directions) at two frequencies we were able to construct the synthetic maps of rotation measures (RM) as well. In the RM calculations we apply the density of gas taken directly from our simulations. A cut of the rotation measure distributions along the major axis of both modeled at four different time steps and observed galaxy (NGC 5775) for comparison are presented in Fig. 7. Our models reproduce the general trend of the rotation measure. The deviations – most prominent jumps around 6 kpc of both sides coincide with the narrow depolarized canals on the polarized intensity map (Fig. 6 – upper panel), where the polarization vectors change their direction rapidly (that leads to large uncertainties of RM determination). Other differences between the model and observations (in the center and at the peripheries) are possibly caused by non-axisymmetries in magnetic field and thermal gas distribution (such as spiral arms), certainly present in NGC 5775 and not included in our model.

5. DISCUSSION

The extended structures appear in the modelled galaxy as a result of variety of physical processes. First of all, the buoyancy driven by CRs transports the magnetic field together with CR gas to the halo. We find that the winds in halo build the vertical magnetic component. Those winds reach speeds up to 100 km/s) and form quickly at the beginning stage of (see Hanasz et al. 2004).

Our local-box simulations show excessive energy density of CRs with respect to the magnetic energy. Possible reasons of this deviation from equipartition are the reduced CR parallel and perpendicular diffusion coefficients and the assumed horizontal periodicity of the computational domain. The latter assumption leads to trapping of CRs by the horizontal magnetic field. (see Hanasz et al. 2008).

Nevertheless, for the first time we apply the modeled CR distribution to perform calculations of the polarized emission in our modeled galaxy. The obtained results are in large extent in agreement with observations. The model presented in this paper demonstrates that, even if the modeled disk starts from 2 kpc from the center of the galaxy, the magnetic field still can take the form of X-shaped structures in the halo.

The maps of face-on model show that the pitch angles of the polarization vectors are about 5° . This value is a bit smaller than the angles usually observed in the spiral galaxies. We underline the fact, however, that our model does not take into account effects of spiral arms in the galaxy. The arms understood as manifestation of density waves are known to influence the magnetic field structure in galactic disks significantly (Beck & Hoernes 1996).

Our model calculates polarized intensity only. It does not include any turbulent structures below relatively large grid size (20, pc). This results in lack of total power emission map comaprable with real observations. It does not allow any reasonable discussion of depolarization other than caused by beam smoothing and/or Faraday effects.

The Faraday effects computed in our model does not influence the overall results. Differences between the rotation measure model and observations are certainly due to limitations of axisymmetric model imposed by extending the local-box into the global galactic model.

One could make the final picture more realistic via the incorporation of supernova remnants. The incorporation of heat output from supernovae may lower the cosmic ray excess. We suggest that global simulations of cosmic ray-driven dynamo may solve the problem as well, however both mentioned solutions of the CR excess problem require much larger computational resources and other numerical algorithms than those currently available for our project. It seems however that the large-scale qualitative features, namely the X-type structures can be succesfully reproduced with the present setup. Therefore we would prefer to demonstrate the observational properties of our present incomplete model of cosmic-ray driven dynamo, rather than to mix quantitative solutions with parametrized effects of supernova remnants. In the present simulations with the shearing box approximation, it is not yet possible to model the vertical shear presumably taking place in the case of NGC 5775 galaxy (Tüllmann et al. 2000). Therefore the global CR-MHD simulations of galactic disks free of limitations of the shearing box should be addressed in the next step of

development of our models.

Five galaxies NGC 891, NGC 3628, NGC 4217, NGC 4666, and NGC 5775 out of six shown in Soida (2005) characterized by the X-shaped structures of magnetic field configuration, have flat rotation curve (Sofue 1996; Rhee & van Albada 1966; Mathewson et al. 1992; Heald et al. 2007). One case (NGC 4631) exhibits different magnetic field orientation with field lines crossing the disk plane. This galaxy also is different when the rotation curve is taken into consideration. It rotates rigidly to the large radii (de Vaucouleurs & de Vaucouleurs 1963). The lack of differential rotation favors development of vertical structures at all galactic altitudes and reduces the speed of transformation of the radial component of magnetic field into the azimuthal one Siejkowski (2008). We suggest that the peculiar structure of the polarized emission which is observed in NGC 4631, where vectors cross the disk plane, can result from the cosmic-ray driven dynamo. This statement is supported by a number of observations Soida et al. (2008). The galaxy NGC 4631 drew our attention and we plan to consider it in our future research.

6. CONCLUSIONS

In the present paper we compare the maps of polarized synchrotron radio emission of galaxy NGC 5775 with those constructed from the numerical model of the cosmic ray driven dynamo. The main conclusions can be summarized as follow:

- All models of the local cosmic-ray driven dynamo computed at the galactic radii between 4kpc and

10kpc indicate the fast growth of the magnetic flux and the total magnetic energy.

- The synthetic radio maps of polarized emission computed on the basis of our local models exhibit vertical magnetic field structures similar to those observed in numerous edge-on galaxies.
- The polarization vectors in the disk plane (face-on) form a spiral pattern with the pitch angles about 5° . The pitch angles from the model are slightly smaller than we normally observe in galaxies. However, the pitch angle of the mean magnetic field depends to some extent on the actual parameters like e.g. the magnitude of the CR diffusion coefficients.
- As it was expected for observation at relatively high frequencies, the Faraday effects considered in our model have no significant importance on the final results.
- The major simplification of our model is caused by assumed axial symmetry, which is necessary for construction of the global model from local-box simulations.

This work was partly supported by the Polish Ministry of Science and Education through the grants: 0656/P03D/2004/26 and 2693/H03/2006/31. Our collaboration has been supported by Polish Ministry of Science and Education through the grant ASTROSIM-PL.

REFERENCES

- Beck, R. and Hoernes, P., 1996, *Nature*, 379, 47
- Berezinskii, V.S., Bulanov, S.V., Dogiel, V.A., Ginzburg, V.L., Ptuskin, V.S., *Astrophysics of cosmic rays*, Amsterdam: North-Holland, 1990.
- Dahlem, M., Petr, M. G., Lehnert, M. D., Heckman, T. M., Ehle, M., 1997, *A&A*, 320, 731
- Dumke, M., Krause, M., Wielebinski, R., Klein, U. 1995, *A&A*, 302, 691
- Ferrière, K.M. 1998, *ApJ*, 497, 759
- Giacalone, J., Jokipii, R.J. 1999, *ApJ*, 520, 204
- Gressel, O., Elstner, D., Ziegler, U., Rüdiger, G. 2008, *A&A* 486L, 35
- Gressel, O., Ziegler, U., Elstner, D., Rüdiger, G. 2008, *AN*, 329, 619
- Hanasz, M. & Lesch, H. 2000, *ApJ*, 543, 235
- Hanasz, M., Otmianowska-Mazur, K. & Lesch, H. 2002, *A&A*, 386, 347
- Hanasz, M. & Lesch, H. 2003, *A&A*, 412, 331
- Hanasz, M., Kowal, G., Otmianowska-Mazur, K. & Lesch, H. 2004, *ApJ*, 605, L33
- Hanasz, M., Lesch, H., Otmianowska-Mazur, K. & Kowal, G. 2005, *Proc. of the MPGE 2004*, Jagiellonian University Press, 162
- Hanasz, M., Otmianowska-Mazur, Kowal, G., K. & Lesch, H. 2006, *AN* 2006, AN 327, 469
- Hanasz, M., et al. 2008, *A&A* (submitted)
- Hawley, J. F., Gammie, C. F. & Balbus, S. A. 1995, *ApJ*, 440, 742
- Heald, G. H., Rand, R. J., Benjamin, R. A., Collins, J. A., Bland-Hawthorn, J. 2007, *ApJ*, 636, 181
- Heesen, V., Krause, M., Beck, R., Dettmar, R.-J., 2005, *Proc. of the MPGE 2004*, Jagiellonian University Press, p. 156
- Jokipii, J. R. 1999, in J. Franco and A. Carraminana (eds.), *Interstellar Turbulence*, Cambridge University Press, 70–78
- Kowal, G., Hanasz, M., Otmianowska-Mazur, K., 2003, *A&A*, 404, 533
- Longair M.S., 1994, *High energy astrophysics*, Cambridge University Press, Cambridge
- Mathewson, D. S., Ford, V. L., Buchhorn, M., 1992, *ApJS*, 81, 413
- Otmianowska-Mazur, K., Kowal, G., Hanasz, M., 2007, *ApJ* 668, 110
- Parker, E. N. 1992, *ApJ*, 401, 137
- Rhee, M.-H., and van Albada, T. S. 1996, *A&AS* 115, 407
- Ryu, D., Kim, J., Hong, S. S., Jones, T.W., 2003, *ApJ*, 589, 338
- Shukurov, A. 2000, *Proc. 232 of WE-Heraeus Seminar*, Shaker, Aachen, 2000, p. 191
- Siejkowski, 2008, in prep.
- Sofue, Y. 1996, *ApJ*, 458, 120
- Sokoloff, D. D., 2002, *ARep*, 46, 871
- Soida, M. 2005, *Proc. of the MPGE 2004*, Jagiellonian University Press, p. 185
- Soida et al., 2008, *A&A* submitted
- Stone, J. M. & Norman, M. L., 1992a, *ApJs*, 80, 753
- Stone, J. M. & Norman, M. L., 1992b, *ApJs*, 80, 791
- Sukumar, S., Allen, R. J., 1991, *ApJ*, 382, 100
- Tanuma, S., Yokoyama, T., Kudoh, T., Shibata, K. 2003, *ApJ*, 582, 215
- Tüllmann, R., Dettmar, R.-J., Soida, M., Urbanik, M., Rossa, J., 2000, *A&A* 364, L36
- de Vaucouleurs, G and de Vaucouleurs, A. 1963, *ApJ*, 137, 363